Time-resolved and spectrally resolved ionization with a single ultrashort XUV-IR beamline

V. Loriot, L. Quintard, G. Karras, A. Marciniak, F. Catoire, M. Hervé, I. Compagnon, G. Renois-Predelus, B. Schindler, B. Concina, et al.

Time resolved and spectrally resolved ionization with a single ultrashort XUV- IR beamline

V. Loriot[1], L. Quintard[2], G. Karras[1], A. Marciniak[1], F. Catoire[2], M. Hervé[1], I. Compagnon[1], G. Renois-Predelus[1], B. Schindler[1], B. Concina[1], G. Celep[1], R. Brédy[1], C. Bordas[1], F. Lépine[1] and E. Constant[1,2]*

[1]*Univ Lyon, Université Claude Bernard Lyon 1, CNRS, Institut Lumière Matière (ILM), F-69622 Villeurbanne, France*

[2]*Université de Bordeaux, CNRS, CEA, Centre Laser Intenses et Applications (CELIA), 43 rue P. Noailles 33400 Talence, France*

*Corresponding author: eric.constant@univ-lyon1.fr

Abstract: We present a simple upgrade of a time resolved attosecond XUV-IR setup designed to perform time resolved or spectrally resolved studies of a target under similar experimental conditions. A flat XUV grating inserted in the path of an attosecond pulse train obtained via HHG in gases is used either in the zeroth order of diffraction to follow attosecond dynamics or in the first order of diffraction to study the target spectral response with a temporally stretched single harmonic. Electron momentum measurement is performed with a Velocity Map Imaging (VMI) spectrometer and the 10 W femtosecond laser system operating at 5kHz provides an XUV photon flux compatible with rapid acquisition in both the monochromatic and broadband configurations. The change of experimental configuration between broadband and monochromatic sources is rapid and performed *in situ*. We present the experimental implementation applied to Krypton atoms and detail the capabilities and limits of this approach when an XUV grating with constant groove density is used with a converging XUV beam.

OCIS numbers: Multiharmonic generation (190.4160), Ultrafast nonlinear optics (190.7110), Ultraviolet extreme (260.7200), Monochromator (120.4140)

1. Introduction

Time resolved experiments using attosecond pulses have demonstrated their ability to measure electron dynamics on its natural timescale and attosecond processes can now be studied using state-of-the-art attosecond beamlines [1-4]. The use of attosecond pulses naturally implies the use of a broadband coherent extreme ultraviolet (XUV) light involving photon energies above the usual ionization potential of atomic, molecular or solid sates target. The interaction of these photons with these targets is highly energy dependent as observed in synchrotron measurements. Hence, to interpret time resolved measurements at the attosecond timescale, it is often necessary to measure the spectral dependence of the interaction. For that purpose, several beamlines devoted to temporally and spectrally resolved experiments using the same setup have emerged with different strategies. A first strategy consists in selecting a range of XUV photons energy using a combination of XUV filters [5] or specifically designed XUV mirrors [6]. Another strategy consists in controlling the XUV spectra with gratings. Dual-gratings time compensated monochromators [7-9] or monochromators using single grating with conical diffraction [10] have been developed. These strategies provide the spectral response of a system and they have the advantage of preserving short pulses while controlling the XUV spectra. Therefore, they provide simultaneously time resolved and spectrally resolved resolution. However, XUV filters and mirrors do not easily allow arbitrary selection of photon energy and XUV monochromators delivering short pulses (time compensated or relying on conical diffraction) remain complex systems that require precise alignment. In the present paper, we investigate the performances and limitations of a simple alternative that allows for performing broadband time resolved experiments with ultrashort pulses and spectrally resolved experiments (here, without temporal resolution) using a single setup. In this approach, a flat XUV grating with grooves perpendicular to the XUV

propagation axis is inserted in the path of the converging XUV beam. By rotating the grating *in situ* to use it either in the 0^{th} order or the 1^{st} diffraction order, it is possible to switch rapidly between two configurations where broadband XUV light (0^{th} order) or narrow band XUV light (1^{st} order) can be used.

In this paper, we explore this scheme as a solution to perform temporally and spectrally resolved studies in a single setup. This provides complementary information on a given target under nearly identical experimental conditions since the same experimental system (target injection, detection system, etc) can be used in both configurations without any change on the beam path after rotating the grating. The spectrally resolved responses often present little interest with atomic systems that have only few active electronic states in a limited spectral range. However, it is an important complement to the time resolved response when complex systems are studied since a large number of states can be accessible. Performing spectrally resolved studies can provide direct information, for each photon energy, on the energy and population of the states involved in the dynamics studied in the broadband configuration. We describe the harmonic generation setup and then present in detail the experimental possibilities in the temporally or spectrally resolved configurations. We illustrate our approach by using Krypton (Kr) atoms. First, we perform spectrally resolved photoionization experiments with isolated single harmonic in the narrowband configuration. Second, we use broadband XUV light to show that the attosecond structure of the XUV pulses is preserved in the broadband configuration and we measure scattering delays in photoionization of Kr at the sub-10 attosecond level. Characterisation of the performances of the experimental setup is performed in both configurations.

2. Experimental setup.

The experimental setup is shown in figure 1. It relies on a commercial femtosecond laser (Legend Elite Duo from Coherent®) delivering 2 mJ, 25 fs pulses centred around 800 nm at a repetition rate of 5 kHz. The laser beam is split into two parts of unequal amplitudes. The main part of the laser beam, is used to create an ultrashort XUV pulse via high order harmonic generation (HHG) in a gas cell located under vacuum. The laser beam is clipped by an iris and focused with a 30 cm focal length lens. Near the focus, the harmonics are generated inside a 5 mm long gas cell closed with two Teflon windows (1 mm thickness) that are drilled *in situ* by the laser beam.

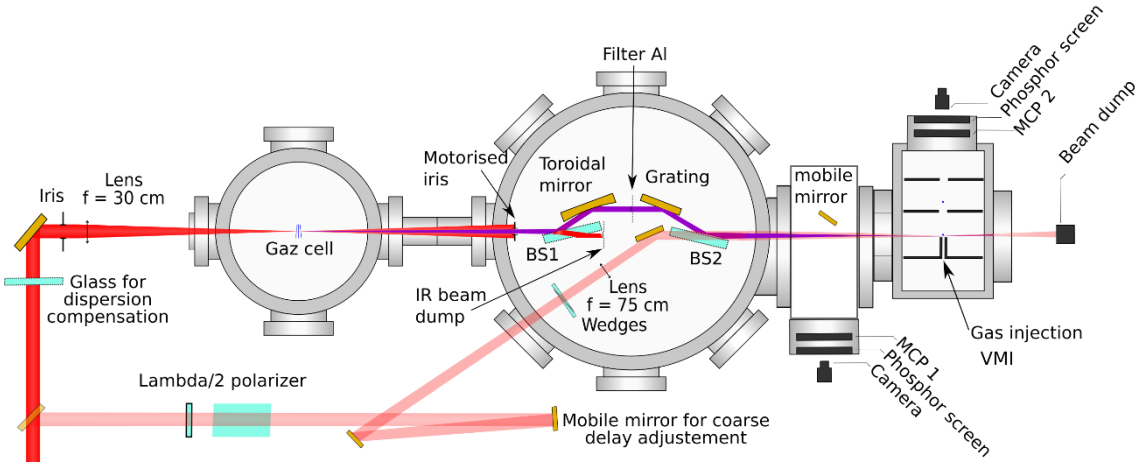

Fig. 1. Sketch of the experimental setup. The harmonic generation chamber (left) contains a 5 mm long gas cell , a second chamber (center) is devoted to the control and focusing of the XUV and IR beams and to their recombination. These chambers are followed by a removable optical XUV spectrometer and a velocity map imaging spectrometer (right).

After harmonic generation, the XUV beam is transmitted via a differential pumping tube and clipped by an iris to limit its divergence. The XUV light is then reflected by a super-polished fused silica plate (BS1 on figure 1) at 70° incidence angle. This plate is coated with an antireflection coating at 800 nm having a thin Nb_2O_5

uppermost layer to reflect the S polarized XUV light with an estimated efficiency of ~50% [11, 12] and to transmit the main part of the IR laser beam. The XUV light is then reflected by a gold coated toroidal mirror with 30 cm focal length used at 70° incidence angle and designed to image the XUV source in the sensitive zone of a velocity map imaging (VMI) spectrometer with a magnification factor of ~1.5. An optional aluminium filter can be inserted into the beam to filter out the fundamental beam and the low order harmonics. The converging harmonics are reflected (zeroth order of diffraction) or diffracted (first order of diffraction) by a flat gold coated grating with 600 grooves / mm. The grating, used with grooves perpendicular to the laser propagation axis, is mounted on a motorized rotation stage that controls the incidence angle, *i*, of the XUV light on the grating. It induces a deviation of $D = 134.1°$ and allows the selection of the reflected light (specular reflection in the zeroth order of the grating for $i = 67°$) or the diffracted light (+1 and -1 diffraction orders around $i = 69°$ and $i = 65°$) by changing the incidence angle. This approach allows using the XUV light as an attosecond pulse train reflected in the zeroth order of the grating for high temporal resolution or using the XUV light diffracted in the +1 grating diffraction order for spectral selectivity. The two configurations can be selected *in situ* without changing the axis of the outgoing XUV beam. After the grating, a second Nb_2O_5 coated beam splitter (BS2 on Fig. 1) reflects the XUV light toward the interaction zone of a VMI spectrometer.

For compactness and flexibility of the setup, we use four reflections on XUV optics and moderate grazing angles. The optics have a reflectivity that is reasonable for the XUV spectral range (typically 50 %) but the four reflections limit the transmission of the ensemble to a few percent or even about one percent when the aluminum filter is used. This prevents the use of very high order harmonics that have lower reflectivity. Nevertheless, our system is compact and robust and we show here that it is compatible

with the rapid recording of the time resolved and spectrally resolved responses of a system in a spectral range of high interest for molecular or solid states studies.

The XUV spectrum is measured by inserting a gold mobile mirror at 45° incidence angle on the XUV beam path before the VMI. The mirror reflects the XUV beam [12] that focuses on a dual microchannel plates (MCP1 on figure 1) detector with phosphor screen that is imaged with a CCD camera. The XUV spectrometer can be used to characterize the XUV spectrum with both the +1 and -1 orders of diffraction of the grating and is used to maximize the harmonics signal.

The XUV pulse can be recombined with a delayed 800 nm infrared (IR) 25 fs probe pulse and the IR pulse energy is controlled by a half wave plate and a thin polarizer. The XUV-IR delay is controlled with sub-100 as accuracy with a pair of fused silica wedges (4° angle) inserted inside the IR beam path. One wedge is installed on a motorized translation stage and the two wedges assembly is equivalent to a glass plate of controllable thickness. The few 100 µm thickness variation required to control the delay over hundreds of fs is small enough so that it does not significantly change the IR pulse duration. The recombination of the XUV and IR beams is performed by transmitting the IR beam and reflecting the XUV beam on a beamsplitter (BS2 on Fig.1). The beamsplitter has the advantage to preserve a smooth spatial profile for the IR beam in contrast to the standard approach based on a holed mirror that transmits the XUV and reflects an annular part of the IR beam. Moreover, the focusing of an annular beam produces localized over intensities [13] and creates a complex phase advance near focus [14]. Such effects can be problematic for instance for characterizing and using attosecond pulses and they are avoided here with the use of an XUV-IR beamsplitter.

After recombination, the XUV and IR beams co-propagate toward the interaction region of a VMI spectrometer that has been specifically designed so that the XUV light

can interact with high pressure gas jet to maximise the electron signal. In this configuration inspired by the VMI described in [15], the XUV beam can be focused few hundreds of microns away from the 50 µm diameter gas injection hole.

3. Experimental results and discussion.

A. Characterization of the XUV source and selection of a single harmonic

High order harmonics produced by a many cycle laser pulse result in a comb of odd harmonics with amplitudes that depend on many parameters such as the gas medium length and position, the gas species, the pressure, the laser peak intensity and pulse duration [16 - 19]. All these parameters are optimised to maximise the harmonics peak brightness on the XUV spectrometer. The spectrometer is calibrated by scanning the grating angle, θ, and recording the XUV spectrum for both orders of diffraction +1 and -1 (figure 2) with a constant deviation, D, that is imposed by the grating and detector positions. The diffraction efficiency can change with the grating angle but the XUV spectrum must exhibit peaks at the same wavelengths in the +1 and – 1 orders. The observed frequencies are odd multiples of the fundamental frequency and are diffracted according to the grating law:

$$\sin(i) = \sin(r) + m\,\lambda / d \qquad (1)$$

(where λ is the XUV wavelength, r is the diffraction angle, m = ±1 the orders of diffraction, $d = 10^{-3}/600$ m the groove separation distance).

For a constant deviation, D, this formula can be written as:

$$Sin\,(\theta) = \frac{\lambda}{2d\,Cos(\frac{D}{2})} \qquad (2)$$

with

$$i = D/2 - \theta \qquad (3)$$

and

$$r = D/2 + \theta \tag{4}$$

The frequencies are not evenly distributed as a function of the grating angle θ (figure 2) and the positions of the peaks measured in the orders of diffraction $m = \pm 1$ are only compatible with a specific assignment of the harmonic orders. This approach provides the exact incidence angle on the grating and the exact deviation (D=134.1°) that are usually difficult to measure experimentally. It provides a robust calibration of the XUV wavelength as shown on figure 2 where the calibration is expressed in terms of harmonic orders. This figure also exhibits extra peaks around the low order harmonics that correspond to the second order of diffraction of the higher order harmonics.

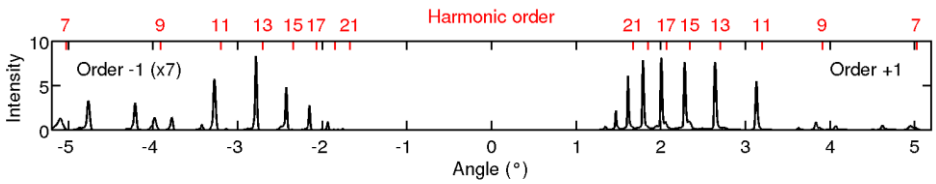

Fig. 2. XUV spectrum measured as a function of the grating angle, θ, for diffraction orders ±1 (order -1 intensity is multiplied by 7) and harmonics generated in krypton gas. Sharp harmonic peaks are observed corresponding to odd harmonics of the fundamental frequency. The angle $\theta = 0$ denotes the position where the XUV beam reaches the detector after specular reflection (not shown here).

This spectrometer allows observing discrete harmonic peaks but it may also be interesting to measure the spectral content of each harmonic. When a grating with constant groove is used, the resolution can be impacted by aberrations due to the divergence of the XUV beam. Using a non-collimated XUV beam implies that the incidence angle on the grating changes inside the beam profile because of the curvature of the wavefront [20-21]. For monochromatic light, a spread, δi, in the incidence angle distribution implies a spread $\delta\theta$

in the grating angle and a spread δr in the diffracted angle distribution. It leads to a broadening of the harmonics that limits the spectral resolution.

Differentiating the equation (3) and (4) leads to:

$$-\delta i = \delta r = \delta\theta \tag{5}$$

That shows that a distribution in the incidence angles leads to the same distribution in the grating angles. From eq. 2, we obtain that the broadening due to the divergence is:

$$\delta\lambda = \delta\theta \, 2d \cos(\theta) \cos\left(\frac{D}{2}\right) \tag{6}$$

showing that the resolution evolves as a function of the photon energy via θ and becomes worse for the highest harmonic orders. The measured width of the harmonics and the sources of broadening are presented in Figure 3. The widths of the harmonics are measured between 120 meV and 400 meV. The δE = 120 meV minimal width implies that the HHG process lasts for at least τ = 15 fs as estimated for Gaussian pulses with the uncertainty relation $\delta\nu \, \tau = 0.441$ where $\delta E = h \, \delta\nu$. As discussed above, the geometrical aberrations are also responsible for a broadening of the signal, which has an impact especially on the highest harmonics. We obtain a good agreement between the measured values and the simulations by considering a constant harmonic width of 120 meV and the broadening associated to a divergence of 250 µrad. This is shown in Figure 3 where both contributions appear for several values of the divergence of the XUV beam and where the estimated total width is the square root of the sum of the two contributions squared. This analysis shows that the resolution of the spectrometer is limited by geometrical aberrations for harmonic orders above 15 and that the spectral content is correctly estimated for lower orders harmonics. To overcome this resolution limitation, grating with variable grooves density [20, 21] can also be used but here we focus on the simpler case of a grating with constant groove density. We conclude that this design is well adapted to the observation of discrete harmonic peaks. With an XUV pulse duration

estimated to 15 fs, it provides a correct estimate of the harmonic spectral width for harmonics with orders $q \leq 13$ and the measurement is limited by the geometrical aberrations for higher harmonic orders.

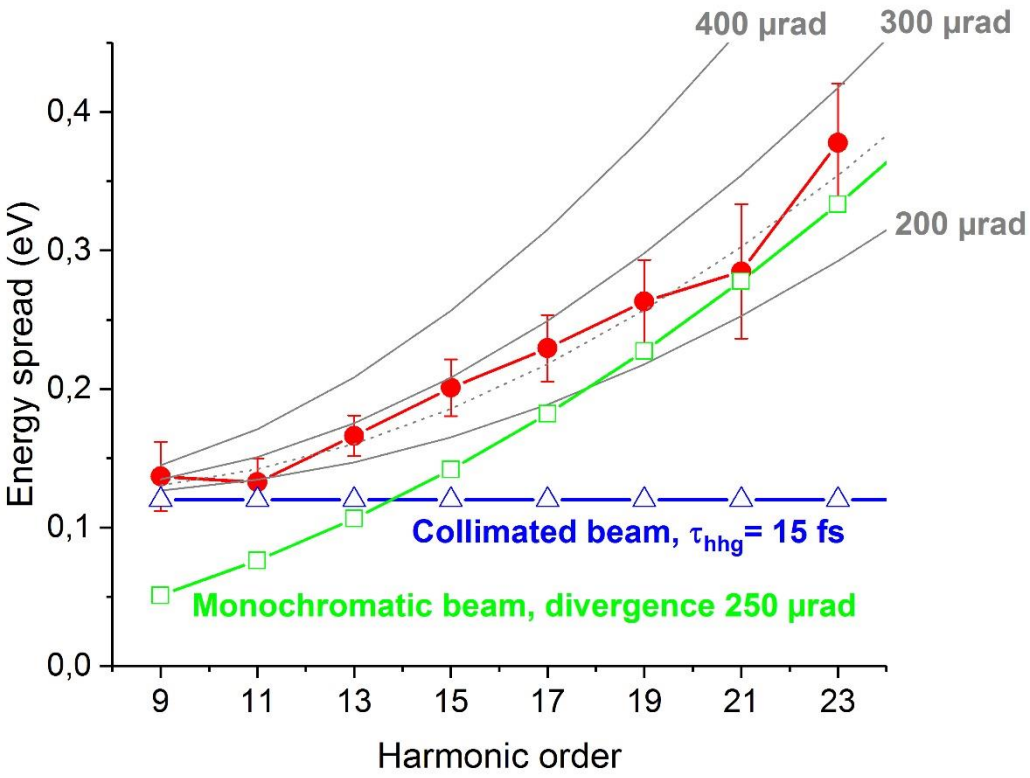

Fig. 3: Measured (red full dots) and simulated (grey lines) energy spread of the XUV comb for several values of the divergence (200, 300 and 400 µrad: full lines, 250 µrad: dotted line) of the XUV beam incident on the grating. The minimum energy spread imposed by the finite duration of the HHG process (blue open triangles) is shown for a harmonic duration of 15 fs. The energy spread due to geometrical aberrations for a divergence of 250 µrad for monochromatic harmonics is represented with open squares

symbols. The measured data is an average over six data sets and the error bar is the standard deviation.

B. VMI Photoelectron detection using isolated harmonics or broadband XUV light

As presented above, full or individual harmonics can be routed to the VMI by rotating the XUV grating and removing the mirror to the spectrometer. Such pulses can be used to ionize atoms in the interaction zone of the VMI spectrometer. The broadband XUV illumination of the target is obtained by tuning the grating to the zeroth order diffraction and removing the residual IR pulse using an Al filter. Single harmonics are selected by tuning the grating to the corresponding diffraction angle. In that case, the aluminium filter can be removed since the residual IR pulse is no longer co-propagative with the XUV light at the first order of diffraction. The selection of a single harmonic is ensured by inserting a 6 mm diameter iris at the entrance of the VMI. Without this iris, several harmonics would enter the VMI and create background noise photoelectron signal. In this study the VMI and the jet axis direction are perpendicular to the laser propagation axis and in the grating diffraction plane.

A demonstrative study is performed by injecting Kr gas in the VMI and recording photoelectron momentum distributions as shown in Figure 4. This measurement shows that the XUV photon flux and gas density are sufficient to create a high photoelectron signal with the broadband illumination despite the limited transmission of the Al filter (see table 1) that was used to block the low harmonics and despite the four reflective XUV optics. When using the first order of diffraction, the photon flux was also significant despite the limited grating diffraction efficiency (see table 1). In both cases, the

acquisition time of a VMI image was on the order of 10 seconds which is compatible with parametric studies.

Figure 4 shows VMI images after Abel inversion obtained with Kr target ionized in broadband (fig. 4 g) and narrowband (fig. 4 a – f) configurations. The inverted VMI images are composed by concentric rings where the radius corresponds to the electron momentum modulus and the angular distribution to the anisotropy of the ionization process [22-23]. The electron momentum distribution depends on the XUV spectrum and on the electronic structure of the gas target as the photoelectron energy is equal to the energy of the absorbed XUV photon minus the ionization potential of the initial state of the target (and possibly minus the residual internal energy when the ion remains in an excited state). With broadband illumination of Kr gas, we observe several concentric rings while only a single (or double) ring is detected with narrowband illumination. The figure 4 (a – f) shows the signal evolution when the harmonics 11 (17 eV) to 21 (32 eV) are successively selected. In this configuration, we observe that the ring diameter increases with the order of the selected harmonic as expected.

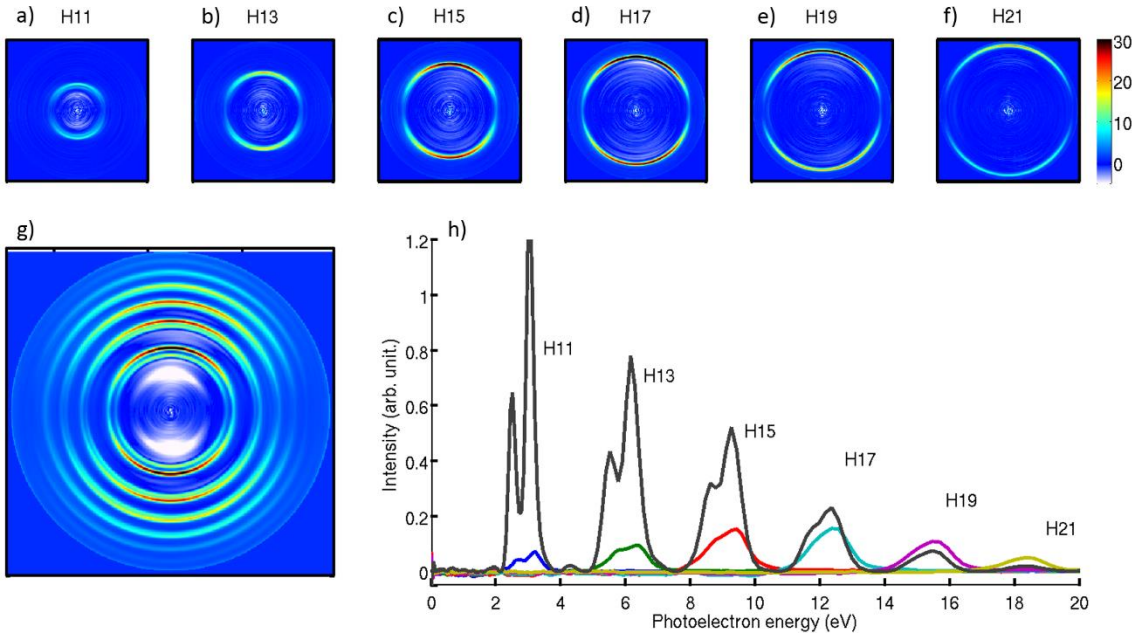

Fig. 4. Velocity map images obtained on Kr target after Abel inversion. Images (a-f) are obtained after selection of isolated harmonics with orders q = 11 to 21 and narrowband illumination of the gas. The (g) VMI image is obtained with broadband illumination of the Kr gas. The photoelectron energy spectra, obtained after angular integration of these images over an angle of ±25°, are shown on the bottom right (h) for both a broadband illumination (black curve) and a spectrally resolved illumination (coloured curves).

We consider the photoelectron energy spectrum after integration of the signal over an angle of ±25° where the signal is maximum (Figure 4). We observe that the peaks are separated by 3.1 eV which is the energy separation between consecutive odd harmonics generated with an 800 nm fundamental laser. The low energy peaks are split into two sub-peaks separated by 0.7 eV. They are due to the spin-orbit splitting in Kr^+ that leads to two cationic states with ionization potentials of 14.00 eV ($^2P_{1/2}$ state of Kr^+) and 14.67 eV ($^2P_{3/2}$ state of Kr^+). With broadband irradiation, the two spin-orbit components are clearly visible in the first three harmonics peaks but they are blurred for the higher order ones. The loss of resolution for high energy electrons is due to the resolution of the VMI ($\Delta E/E = 9\pm1\%$) which decreases with increasing photoelectron energy.

When narrow band illumination is used (Figure 4), the two spin-orbit components are only visible after irradiation with the 11^{th} harmonic showing that the resolution is insufficient to discriminate them when higher harmonics are selected. This reduced resolution is due to the spatial dispersion (spatial chirp and geometrical aberrations) induced by the grating on the diffracted XUV beam. It enlarges spatially the XUV beam near focus and leads to an elliptical focus for each harmonic with an estimated size of 200 µm to 500 µm depending on the harmonic. The energy resolution in a VMI is linked to the spatial extension of the electron/ion source [22-23] and increasing the size of the source leads to the blurring of the peaks. In this configuration, the photoelectrons are created in a large gas volume and the VMI resolution is degraded. We measure a

resolution of $\Delta E/E = 15 \pm 3\%$ for photoelectrons originating from harmonics above 13 and 0.55 eV for the peak associated to the electrons originating from harmonic 11.

We use the comparison of the measurements performed in the broadband and monochromatic configurations with full angular integration to estimate the relative diffraction efficiency of the grating. This efficiency is usually difficult to estimate in the XUV but it can be conveniently measured with this setup. The angle of incidence is weakly changed between broadband and monochromatic measurements and we assume that the diffraction efficiency, η_q, changes only weakly and does not modify the spectrum of the specular reflection. If we consider that the gas density is constant in the interaction zone, the integrated signal originating from one harmonic with spectral selection ($S_q^{\text{order 1}}$) in a given diffraction order is a fraction of the total XUV signal (S_q^{tot}). It can be written as:

$$S_q^{\text{order 1}} = \eta_q \, S_q^{\text{tot}} \tag{7}$$

The signal remaining in the zeroth order is close to the signal detected in the broadband configuration after dividing this signal by the measured Al filter transmission (Table 1). It can be expressed as the total incoming signal minus the signal diffracted in the order +1, -1 and other orders. In the simplified condition where a single order of diffraction is predominant, we obtain the diffraction efficiency for this order:

$$\eta_q = S_q^{\text{order 1}} / (S_q^{\text{zero order}} + S_q^{\text{order 1}}) \tag{8}$$

The measured diffraction efficiencies are summarized in table 1. They first increase with the harmonic orders with a maximum of 12% for the harmonic 19 and then decrease. This measurement shows that the diffraction efficiency is low and ensures that the XUV spectrum reflected in the zeroth order is similar to the input spectrum.

Harmonic order	11	13	15	17	19	21
Diffraction efficiency	0.5 %	1.5%	4%	8%	12%	10%
Al filter transmission	3.7%	6.8%	11.8%	15.6%	17.4%	16.9%

Table 1: Estimation of the diffraction efficiency measured in the order +1 for the 600 gr/mm gold grating used with a deviation of 134.1° and measured transmission of the 200 nm Al filter.

When a single harmonic is selected, the setup is not optimized for pump-probe measurements because of the limited XUV-IR spatio-temporal overlap. There are two reasons for this limitation. First, there is a limited temporal overlap between the XUV pulse and the IR pulse because XUV pulses are stretched by the spectral selection. The temporal stretch is linked to the number of grooves that are illuminated on the grating by the XUV beam and we estimate that the harmonic pulse duration is approximately stretched by one XUV optical period for each groove that is illuminated [7, 24]. With the XUV beam divergence measured here, approximately 250 grooves are illuminated and the XUV pulse is stretched to around 50 fs (61 fs for the 11^{th} harmonic and 29 fs for the 23^{rd} harmonic) after the grating. Furthermore, the frequency components within one harmonic are angularly dispersed and the frequency components are spatially separated within one harmonic after propagation to the VMI. This reduces the bandwidth locally and further stretches the pulse in the VMI interaction zone implying a limited temporal overlap with a short IR pulse probe. The second reason is the limited spatial overlap between the XUV and the IR beams. This limited overlap is due to the large spatial profile of the XUV beam in the interaction zone imposed by the XUV spatial chirp and the divergence-related geometrical aberrations (Fig. 3). Overall, the XUV spatial profile does not match the spatial profile of the IR beam near focus. This limited spatial overlap would

also lead to a reduction of any XUV - IR pump-probe signal that is proportional to the spatial overlap between the XUV and IR beams.

This design is not optimum for pump-probe studies with isolated harmonics [7 – 10] but we have shown that isolated harmonics can be used to perform spectrally resolved ionization. The capabilities of the spectrally resolved studies were presented here with Kr atoms that exhibit two ionization potentials due to the fine structure of the ion. This spectrally resolved approach is also well suited for more complex targets such as molecules with multiple states that can be simultaneously ionized by broadband XUV irradiation. The ability to decompose a broadband excitation into the sum of several narrow band excitations under nearly identical experimental configuration is a key step to disentangle the contribution of each energy level and harmonic. In the following, we consider the full harmonic comb and show that this approach allows us to perform time resolved measurements with attosecond resolution.

C. Attosecond time resolved studies with broadband XUV light

The experiment is designed to perform also XUV-IR time resolved studies by irradiating the sample with the XUV light reflected by the grating in the zeroth order and a delayed short IR pulse. In this case, the grating acts as a mirror that weakly affects the XUV spectrum when the diffraction efficiency is low as observed here. In principle, the zeroth order reflection on a grating should not affect the attosecond structure of the XUV pulse train but experimental evidence is needed to confirm this point. For that purpose, we perform RABBITT [25] measurements that consists in measuring the evolution of two-color photoelectron spectrograms as a function of the XUV-IR delay. Such spectrograms are shown in figure 5 for both Ar and Kr targets. The full scans were obtained with a typical acquisition time of 20 minutes. For large delays, the XUV and IR pulses do not overlap temporally and the spectra exhibit bands of energy that are

characteristics of the absorption of one harmonic photon only. For short delays when pulses overlap, additional energy bands (sidebands) appear between the former peaks and are due to the simultaneous absorption of an XUV photon and absorption or stimulated emission of an IR photon. The amplitude of the sidebands changes with the delay on both long (~30 fs) and short (~1 fs) time scale. The long time scale evolution is linked to the cross correlation between the XUV pulse and the IR pulse envelops. On shorter time scales, regular oscillations appear with a period of 1.33 fs. These experimental results show contrasted oscillations that are the signature of a high stability of the IR-XUV delay obtained here without any active stabilization system [26]. The phase of these oscillations is related to the phase shift between consecutive harmonics plus a small additional factor called atomic phase that depends on the properties of the atomic state involved in the ionization process. The harmonic phases change with the harmonic order as shown in Figure 6.b where the time resolved signal is presented for three sidebands and the two cationic states. This result shows that the phase of oscillations changes between each sideband and changes only weakly with the final cationic state. Assuming that all harmonic beams are homogeneous with identical spatial profiles, these phases allow reconstructing the temporal profile of attosecond pulses with the so-called RABBITT technique [25] or with alternative reconstruction techniques [27-29]. This measurement shows that the attosecond temporal structure is preserved when the grating is used in the zeroth order of diffraction.

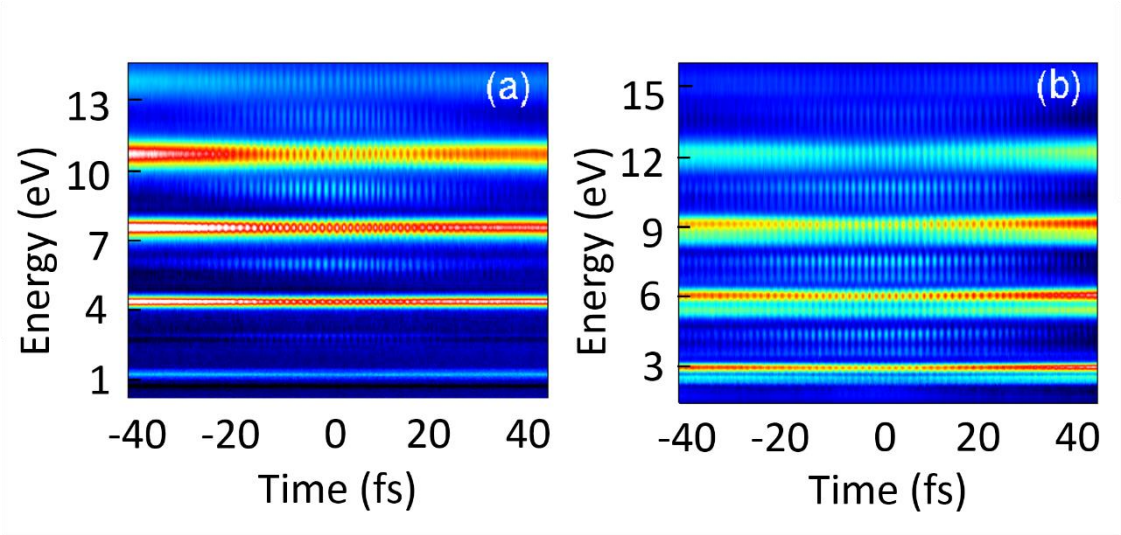

Fig. 5. Time resolved two-color photoelectron spectra obtained as a function of the IR-XUV delay with Argon (a) and Krypton (b) gas.

The photoelectron map obtained with the Kr gas (Fig. 5.b and 6.a) shows harmonic peaks and sidebands that are split into two because of the 0.67 eV spin orbit splitting between the $^2P_{1/2}$ and $^2P_{3/2}$ cationic states. As mentioned above, the oscillations of the sidebands depend on the harmonic phases and also on an additional atomic phase that depends on the atomic state itself. This atomic phase is linked to the scattering phase which can be associated to delays in the scattering of the electron ejected upon photoionization [30-31]. The splitting allows us to extract the oscillation phase of each side band produced by the two cationic states (Fig. 6b) and to measure the relative atomic phases associated to the two final ionic states that provides the relative scattering delay between the two electronic states [30]. In our experiment, the two sidebands are split in two for the sidebands 12, 14 and 16 (Fig. 6a).

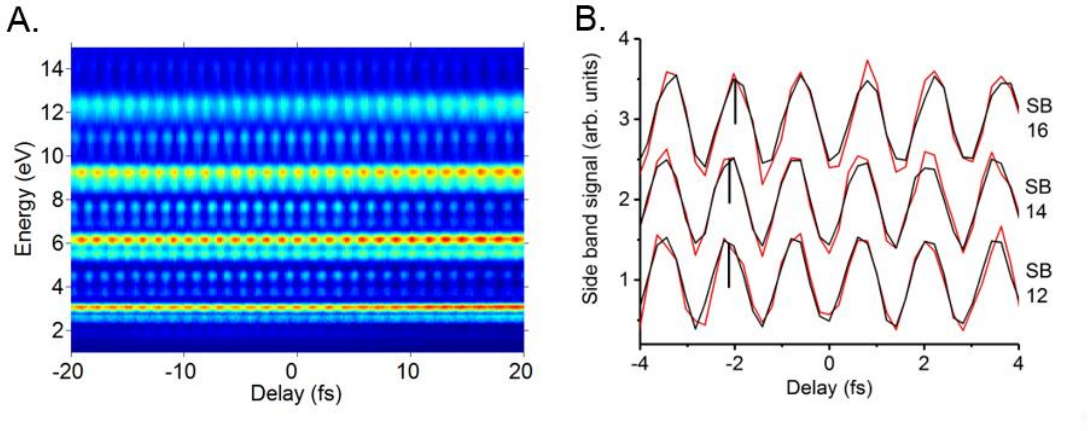

Fig. 6: a/ Photoelectron signal obtained in Kr for XUV-IR delays in the range -20 fs to + 20 fs. b/ Evolution of the sideband (SB) signal integrated over its spectral width as a function of the IR-XUV delay for the sidebands 12, 14 and 16. Each sideband evolution is separated in two curves that correspond to the $^2P_{3/2}$ cationic state (lower energy photoelectrons in each sideband, red curve) and the $^2P_{1/2}$ cationic state (higher energy photoelectrons in each sideband, black curve).

The temporal evolution of the sidebands associated to the $^2P_{3/2}$ and $^2P_{1/2}$ states (figure 6) are very similar. Each sideband has been integrated over energy and its time dependent evolution has been Fourier transformed to provide the position of the oscillation via the phase of the oscillating component for both the $^2P_{3/2}$ and the $^2P_{1/2}$ states. The difference of phase associated to the $^2P_{3/2}$ and $^2P_{1/2}$ sidebands gives the so-called scattering delay after considering that a full period of oscillation is half the optical period of the fundamental light. We measured delays of 11 as for the sideband 12 between the $^2P_{3/2}$ and the $^2P_{1/2}$ states. The delay was 0.6 as for the sideband 14 and of 6 as for the sideband 16 with a standard deviation of 11 as for all these measurements. These values were obtained by limiting the analysis to delays between -20 fs and +20 fs where the signal is maximum and where oscillations show a good contrast. The sideband signal is

then extracted in an 8 fs wide test-window and a Fourier transform is performed to obtain the phases of the oscillations in this window. This provides the relative scattering delay between the two ionization channels in this time-window. Moving the test-window throughout the 40 fs range gives statistics on the measured relative ionization delays and provides the standard deviation on this measurement. The measured values are compatible with recent measurements [31] where sub-8 as delays were measured in Kr^+. Our observations confirm that the spin-orbit state-dependent shifts in ionization delays are very small in Kr for the harmonics used here. This experiment shows that our compact laser-based beamline allows performing experiments in the time domain with high temporal resolution.

4. Conclusion

In this paper, we have shown that XUV time resolved or spectrally resolved ionization experiments can be performed with minor experimental modifications, the two configurations being selected by simply rotating a flat grating located on the XUV beam path. When the grating is used in the zeroth order of diffraction, it acts as a mirror and the low diffraction efficiency in the +-1 order ensures that the reflected spectrum is similar to the input spectrum. Therefore, the attosecond structure is weakly affected by the specular reflection on the grating and time resolved experiments with attosecond resolution can be performed. When the grating is used in the first order of diffraction the harmonics are temporally stretched and the angular dispersion can be used to extract a single harmonic from the harmonic comb and to achieve spectrally resolved interaction

in the sensitive zone of the VMI photoelectron spectrometer. In both configurations, the XUV photon flux and the target density are sufficient to measure the photoelectrons distribution with the VMI with a typical acquisition time of 10 seconds. We have compared the photoelectron spectra obtained with a short broadband XUV source and with a spectrally resolved XUV source where isolated harmonics are selected. We have shown that time-resolved broadband measurement can be complemented by spectrally resolved measurements that can provide important additional information when targets with complex valence bands are studied. Measurements performed *in situ* provide also the diffraction efficiency of the flat XUV grating that is used to control the XUV light. In the time domain, we measure delay-dependent, two-colour photoelectron spectra with attosecond resolution over a large delay range. We have measured IR/XUV delay dependent photoelectron spectra showing oscillations with high stability and observed scattering delays in the photoionization of Kr involving the $^2P_{1/2}$ and $^2P_{3/2}$ cationic states that are smaller than 10 as. Our approach therefore combines a possible spectral selection of a single harmonic and state of the art resolution in the temporal domain with broadband XUV light in a compact and versatile setup. It can be used to study complex systems with high temporal or spectral resolution with minor experimental modifications and this experimental approach can be very relevant to extract accurate information from highly congested signals.

Acknowledgements: We thank E. Mével and E. Cormier for stimulating discussions and J. Maurelli and L. Merzeau for technical support. We acknowledge funding of the CNRS, the Agence Nationale pour la Recherche (ANR-10-BLAN-0428-01 Muses, ANR-09-BLAN-0031-02 Attowave and ANR-16-CE30-0012 Circé), the federation de physique Marie Ampere and the Aquitaine Region (20101304005 and 20131603008).

References:

[1] F. Krausz and M. Ivanov, Rev. Mod. Phys. **81** 000163 (2009), "Attosecond physics".

[2] F. Lépine, M.Y. Ivanov & M.J.J. Vrakking, Nature Photonics, **8**, 195–204 (2014), "Attosecond molecular physics: Fact or Fiction?".

[3] F. Calegari, G. Sansone, S. Stagira, C. Vozzi and M. Nisoli, J. Phys B **49** 062001 (2016), "Advances in attosecond science".

[4] Z. Chang, P. B. Corkum, S. Leone, Josab **33** 1081 (2016), "Attosecond optics and technology: progress to date and future prospects".

[5] M. Huppert, I. Jordan, D. Baykusheva, A. von Conta, and H. J. Wörner, Phys. Rev. Lett. **117** 093001 (2016), "Attosecond Delays in Molecular Photoionization".

[6] C. Bourassin-Bouchet Z. Diveki, S. de Rossi, E. English, E. Meltchakov, O. Gobert, D. Guénot, B. Carré, F. Delmotte, P. Salières, and T. Ruchon, Opt. exp. **19** 3809 (2011), "Control of the attosecond synchronization of XUV radiation with phase-optimized mirrors".

[7] P. Villoresi, Appl. Opt. **38** 6040 (1999), "Time preserving monochromator".

[8] M. Ito, Y. Kataoka, T. Okamoto, M. Yamashita and T. Sekikawa, Opt. Expr **18** 6071 (2010), "Spatiotemporal characterization of single-order high harmonic pulses from time-compensated toroidal-grating monochromator".

[9] L. Poletto, Appl. Opt. **48** 4526 (2009), "Tolerances of time-delay-compensated monochromators for extreme-ultraviolet ultrashort pulses".

[10] F. Frassetto, C. Cacho, C. A. Froud, E. Turcu, P. Villoresi, W. A. Bryan, E. Springate, and L. Poletto, Opt. Expr. **19** 19169 (2011), "Single-grating monochromator for extreme ultraviolet ultrashort pulse".

[11] A. Cabasse, Ch. Hazera, L. Quintard, E. Cormier, S. Petit and E. Constant, J. Phys. B At. Mol. Opt. Phys **49** 085601 (2016), **"**Collection and spectral control of high order harmonics generated with a 50W high-repetition rate Ytterbium femtosecond laser system".

[12] B.L. Henke, E.M. Gullikson, and J.C. Davis. Atomic Data and Nuclear Data Tables **54** 181 (1993), "X-ray interactions: photoabsorption, scattering, transmission, and reflection at E=50-30000 eV, Z=1-92", http://henke.lbl.gov/optical_constants/.

[13] V. Loriot, O. Mendoza-Yero, J. Pérez-Vizcaíno, G. Mínguez-Vega, R. de Nalda, L.Bañares & J. Lancis, Appl. Phys. B **117** 67 (2014), "Fresnel phase retrieval method using an annular lens array on an SLM".

[14] F. Schlaepfer, A. Ludwig, M. Lucchini, L. Kasmi, M. Volkov, L. Gallmann, and U. Keller Opt. Expr. **25** 3646 (2017), "Gouy phase shift for annular beam profiles in attosecond experiments".

[15] O. Ghafur, W. Siu, P. Johnsson, M. F. Kling, M. Drescher, and M. J. J. Vrakking, Rev. Scient. Instr. **80** 033110 (2009), "A velocity map imaging detector with an integrated gas injection system".

[16] C.-G. Wahlstrom, J. Larsson, A. Persson, T. Starczewski, and S. Svanberg, P. Salieres, Ph. Balcou, and Anne L'Huillier. Phys. Rev. A **48** 4709 (1993), "High-order harmonic generation in rare gases with an intense short-pulse laser".

[17] J. P. Brichta, M. C. H. Wong, J. B. Bertrand, H. C. Bandulet, D. M. Rayner and V. R. Bhardwaj, Phys. Rev. A **79** 033404 (2009), "Comparison and real time monitoring of high order harmonic generation in different sources".

[18] P. Salières, A. L'Huillier, and M. Lewenstein, Phys. Rev. Lett. **74** 3876 (1995), "Coherence Control of High-Order Harmonics".

[19] E. Constant, D. Garzella, E. Mével, P. Breger, Ch. Dorrer, C. Le Blanc, F. Salin and P. Agostini, Phys. Rev. Lett. **82**, 1668 (1999), "Optimizing High Harmonic Generation in Absorbing Gases: Model and Experiment".

[20] M. C. Hettrick and S. Bowyer Appl. Opt. **22** 3921 (1983)
"Variable line-space gratings: new designs for use in grazing incidence spectrometers".

[21] L. Poletto, S. Bonora, M. Pascolini, and P. Villoresi, Rev. Sci. Instr. **75** 4413 (2004), "Instrumentation for analysis and utilization of extreme-ultraviolet and soft x-ray high-order harmonics".

[22] T. J. B. Eppink & D. H. Parker. Rev. Sci. Instr. **68** 3477 (1997), "Velocity map imaging of ions and electrons using electrostatic lenses: Application in photoelectron and photofragment ion imaging of molecular oxygen".

[23] C. Bordas, F. Paulig, H. Helm, D.L. Huestis, Rev. Sci. Instr. **67** 2258 (1996), "Photoelectron imaging spectrometry: principle and inversion method".

[24] A. Visco, R. P. Drake, D. H. Froula, S. H. Glenzer, and B. B. Pollock. Rev. Sci. Instr. **79** 10F545 (2008), "Temporal dispersion of a spectrometer".

[25] P. M. Paul, E. S. Toma, P. Breger, G. Mullot, F. Auger, Ph. Balcou, H. G. Muller, P. Agostini, Science **292** 1689 (2001), "Observation of a Train of Attosecond Pulses from High Harmonic Generation".

[26] V. Loriot, A. Marciniak, L. Quintard, V. Despré, B. Schindler, I. Compagnon, B. Concina, G. Celep, C. Bordas, F. Catoire, E. Constant and F. Lépine, Journal of Physics: Conference Series **635,** 012006 (2015), "Resolving XUV induced femtosecond and attosecond dynamics in polyatomic molecules with a compact attosecond beamline".

[27] Y. Mairesse and F. Quéré, Phys. Rev. A **71** 011401 (2005), "Frequency resolved optical gating for complete reconstruction of attosecond bursts".

[28] M. Chini, S. Gilbertson, S. D. Khan, and Z. Chang, Opt. Expr. **12** 13006 (2010), "Characterising ultrabroadband attosecond lasers".

[29] M. Lucchini, M.H. Brügmann, A. Ludwig, L. Gallmann, U. Keller, and T. Feurer, Opt. Expr. **23**, 29502 (2015), "Ptychographic reconstruction of attosecond pulses".

[30] A. L. Cavalieri, N. Müller, Th. Uphues, V. S. Yakovlev, A. Baltuska, B. Horvath, B. Schmidt, L. Blümel, R. Holzwarth, S. Hendel, M. Drescher, U. Kleineberg, P. M. Echenique, R. Kienberger, F. Krausz & U. Heinzmann, Nature **449**, 1029 (2007) "Attosecond spectroscopy in condensed matter".

[31] I. Jordan, M. Huppert, S. Pabst, A. S. Kheifets, D. Baykusheva, and H. J. Wörner, Phys. Rev. A **95**, 013404 (2017), "Spin orbit delays in photoemission".